



Clathrate hydrate formation in NaCl and MgCl₂ brines at low pressure conditions



Yesol Woo^a, Changho Lee^{b,1}, Jae Hak Jeong^b, Dongseon Kim^{a,c}, Jong-Won Lee^d, Yoshitaka Yamamoto^e, Jeasung Park^f, Minjun Cha^{g,*}, Ji-Ho Yoon^{a,b,c,*}

^a Department of Convergence Study on the Ocean Science and Technology, Ocean Science and Technology (OST) School, Korea Maritime and Ocean University, Busan 49112, Republic of Korea

^b Department of Energy and Resources Engineering, Korea Maritime and Ocean University, Busan 49112, Republic of Korea

^c Marine Chemistry & Geochemistry Research Center, Korea Institute of Ocean Science and Technology, Busan 49111, Republic of Korea

^d Department of Environmental Engineering, Kongju National University, Chungnam 31080, Republic of Korea

^e Methane Hydrate Production System Research Group, Research Institute of Energy Frontier, National Institute of Advanced Industrial Science and Technology (AIST), Ibaraki 305-8569, Japan

^f Intelligent Sustainable Materials R&D Group, Korea Institute of Industrial Technology (KITECH), Chungnam 31056, Republic of Korea

^g Department of Energy and Resources Engineering, Kangwon National University, Chuncheon 24341, Republic of Korea

ARTICLE INFO

Keywords:

Clathrate hydrate
Brine
Formation kinetics
Ion exclusion
Raman spectroscopy

ABSTRACT

Hydrate-based desalination (HBD) has been developed to obtain fresh water from seawater in an economic and environmental sustainable manner. As a low-pressure hydrate former for the HBD process, chlorodifluoromethane (R22) hydrates were formed in the pressure range of 1–6 bar under brine environments, aqueous NaCl and MgCl₂ solutions. Synchrotron X-ray diffraction and Raman spectroscopy measurements revealed that the R22 hydrates formed with NaCl and MgCl₂ show structure I and enclathration of R22 molecules into the large cages. These results also confirmed that the salt ions cannot be engaged in the gas hydrate framework, reflecting the ion exclusion behavior for HBD above the eutectic of water and hydrated salts. The formation kinetics of R22 clathrate hydrate in the presence of salts show that both the initial growth rate and pressure drop of the R22 hydrates heavily depend on the salinity of aqueous solutions. A new theoretical approach adopting the transient time-dependent apparent rate constant of hydrate formation with salts was proposed to predict the formation kinetics of R22 hydrates under brine environments, which was in good agreements with the experimental results. These results provide good information for separating ionic compounds from aqueous solutions by hydrate-based separation processes.

1. Introduction

Over the past several decades, demand for fresh water has continuously increased throughout the world as a result of sustained population growth and improved living standards [1–4]. At the same time, the availability of good quality water is central to sustainable development and further improvements in quality of life. Given the limited availability of fresh water resources, and unreliable water quality for industrial and human needs, desalination technologies involving processes to recover pure water from sea water, have attracted considerable attention [5–10]. Fundamentally, desalination technology removes

salts from sea water to provide fresh water, and various approaches have been proposed over the last several decades to accomplish this, with a range of efficiencies, performance and cost.

Gas hydrates are ice-like inclusion compounds comprised of a ‘host’ water-framework and small ‘guest’ molecules such as methane, ethane, carbon dioxide, etc. Hydrate structures are typically categorized based on differences in the size and shape of the hydrate cages. Huge amounts of gaseous molecules can be selectively stored in the hydrate cages [11–23]. For this reason, gas hydrates are currently considered one of the promising functional materials in the energy and environmental fields because of their possible applications for gas storage and

* Corresponding authors at: Department of Energy and Resources Engineering, Kangwon National University, Chuncheon 24341, Republic of Korea (M. Cha) and Department of Convergence Study on the Ocean Science and Technology, Ocean Science and Technology (OST) School, Korea Maritime and Ocean University, Busan 49112, Republic of Korea (J.-H. Yoon).

E-mail addresses: minjun.cha@kangwon.ac.kr (M. Cha), jhyoon@kmou.ac.kr (J.-H. Yoon).

¹ Current address: Korea Carbon Capture and Sequestration R&D Center, Daejeon 34129, Republic of Korea.

transportation [24–27], carbon capture and sequestration [28–32], the selective separation of gas species [33–38], and desalination [39–41].

Among the various desalination approaches, hydrate-based desalination (HBD) technology is a promising method for recovering fresh water from sea water. The key mechanism of the HBD technology is a simple temperature- and pressure-dependent phase transition from liquid to solid. HBD technology is considered a novel method for reducing the energy costs of desalination, and increasing the level of freshwater recovery. In addition, HBD technology is also regarded as an environmental-friendly method because hydrates can be directly formed from seawater under low-temperature and high-pressure conditions [39–41]. However, achieving the appropriate high-pressure condition for gas hydrate formation is a major obstacle to improving hydrate formation efficiency, and accordingly, the development of an efficient way to form gas hydrates under more moderate conditions is one of the key objectives of current research.

The refrigerant chlorodifluoromethane (R22) is widely used as an alternative to highly ozone depleting materials, such as dichlorodifluoromethane (R12) and trichlorofluoromethane (R11). Despite its relatively low ozone depletion potential of 0.055, R22 is still considered to be one of the ozone depleting materials [42,43]. In addition, R22 is regarded as one of the more powerful greenhouse gases due to its global warming potential, which is 1810 times as high as carbon dioxide. For these reasons, controlling R22 using gas hydrates has been studied in several researches [44–49]. R22 is known as a structure I (sI) hydrate former and R22 can only be captured in the large cages of a sI hydrate due to its large molecular size. In addition, the phase equilibrium conditions of R22 hydrates are milder than those of conventional gas hydrates, such as CH₄ or CO₂ hydrates. Controlling R22 using gas hydrates can lead to hydrates with dual hydrate-based functionality, resulting in both R22 capture and an HBD technology [44–49].

To develop a HBD technology using the R22 hydrate, the phase equilibrium conditions of the R22 hydrates in the presence of various salts needs to be determined, as well as the formation kinetics of the R22 hydrate. Chun et al. [44] reported the phase diagram of R22 hydrates in the presence of NaCl, KCl, and MgCl₂, and Karamoddin et al. [49] investigated the kinetics of R22 hydrate formation in the presence of sodium dodecyl sulfate (SDS).

In this study, the crystal structures and guest inclusion behaviors of R22 hydrates in the presence of NaCl and MgCl₂ were identified using X-ray diffraction (XRD) and Raman spectroscopy. To the best of our knowledge, there have been no prior studies of R22 hydrates using Raman spectroscopy, especially under brine environments; to date, only Raman measurements for gaseous, liquid and solid R22 have been reported [50,51]. We investigated the formation kinetics of R22 hydrates in the presence of NaCl and MgCl₂ solutions. This study also provides a new approach for theoretically predicting the formation kinetics of gas hydrates.

2. Material and methods

NaCl and MgCl₂, with a minimum purity of 99.5 and 98 mol %, respectively, were supplied from Sigma-Aldrich. R22 gas with a minimum purity of 99.8 mol % was obtained from Korea Standard Gas Co.

To identify the crystal structures and guest inclusion behaviors of R22 hydrates in the presence of NaCl and MgCl₂, R22 hydrate samples were prepared by the following processes. High pressure reactors were charged with 100 cm³ of aqueous salt solutions, and then, the reactors were immersed in a water bath held at 274 K. The reactors were slowly pressurized by R22 gas up to 5 bar, and after the cell was stabilized, hydrate formation was triggered by vigorously agitating the R22 gas and the aqueous solutions. R22 gas was repeatedly injected into the reactors to maintain the system pressure for hydrate conversion. After the formation reaction was completed, R22 hydrate samples were recovered and ground to a fine powder with of 100 μm sieve. A

customized Raman spectroscopy instrument with a multichannel air-cooled charge-couple device (CCD) detector (Princeton Instruments, PIXIS 100B) was used to investigate the guest inclusion behaviors of R22 molecules in the R22 hydrates with and without salts. A Nd-YAG laser emitting 532 nm with a power of 150 mW was used as the light source. Raman spectra of the solid hydrate samples and solid R22 were measured at atmospheric pressure and 83 K using a microscope stage (Linkam, THMS 600), while Raman spectra of gaseous and liquid R22 samples were measured at 298 K under pressurized conditions using a high pressure cell with a sapphire window. To identify the crystal structures of the R22 hydrate samples, high-resolution synchrotron XRD measurements were performed in the range of 5–125° with a step size of 0.005° and a wavelength of 1.5183 Å at beamline 9B of the Pohang Accelerator Laboratory (PAL). All XRD samples were measured at 90 K to minimize hydrate dissociation.

The formation kinetics of the R22 hydrate in aqueous salt solutions was investigated using high pressure cells with two sight glasses and an actual internal volume of 277 cm³. The temperature and pressure of the cell were measured by a digital thermometer and a pressure transducer with a resolution of 0.1 K and 0.1 bar, respectively. Two high pressure cells were prepared in the formation kinetics experiments; one (cell 1) was charged with 100 cm³ of aqueous salt solutions, and the other (cell 2) was charged with R22 gas up to the desired pressure condition. Then, the cells were immersed into the water bath at 278 K for stabilization. The two cells are connected by a pressure line, and then R22 from cell 2 gas was injected into cell 1 up to 5.2 bar. After the temperature and pressure condition of cell 1 was stabilized, the hydrate formation was triggered by vigorously agitating the contents in the vapor and liquid phases of the cell.

All kinetic experiments were carried out at the stirring rate of 400 rpm using a magnetic drive attached to the top of the cell. The temperature and pressure were monitored and sampled every 5 s by a data acquisition system. The amount of R22 gas consumed during hydrate formation was determined from the pressure-volume-temperature (PVT) relationship of the R22 [52]. After the 1st run of the kinetic experiment was completed, the pressure in cell 1 was reduced to atmospheric pressure for hydrate dissociation. After 1 h of the hydrate dissociation process, a 2nd run of the formation kinetics experiment was repeated using the same procedure.

During the 1st runs of the kinetic experiment, we observed a significant hydrate induction time, which is a stochastic phenomenon. However, we noted that there was no induction time for hydrate formation during the 2nd run of the experiment, due to the memory effect. To avoid the effect of induction time on hydrate formation, we modified our experimental procedure by the following process.

In the modified experimental procedure, the high pressure cell was charged with 100 cm³ of aqueous salt solutions, and immersed in the water bath at 288 K. The cell was pressurized by R22 gas up to 7.8 bar, which is not a hydrate-forming condition. After the temperature and pressure condition in the cell was stabilized, the temperature of the water bath was reduced to 278 K at a continuous cooling rate of 0.2 K/min. Then, the system pressure was adjusted to 5.2 bar, and hydrate formation was triggered by agitation at a stirring rate of 400 rpm. The temperature and pressure were monitored and sampled every 5 s by a data acquisition system. In both the 1st and 2nd runs of the kinetic experiments, when the modified experimental procedure was applied, we did not observe any induction time for hydrate formation.

3. Results and discussion

3.1. XRD and Raman spectroscopic investigation

High-resolution synchrotron XRD was used to identify the crystal structure of the R22 hydrates with and without salts. Fig. 1 shows the XRD patterns of the R22 hydrates formed in pure water (black line), 5 wt% NaCl (red line), and 5 wt% MgCl₂ (blue line) aqueous solutions,

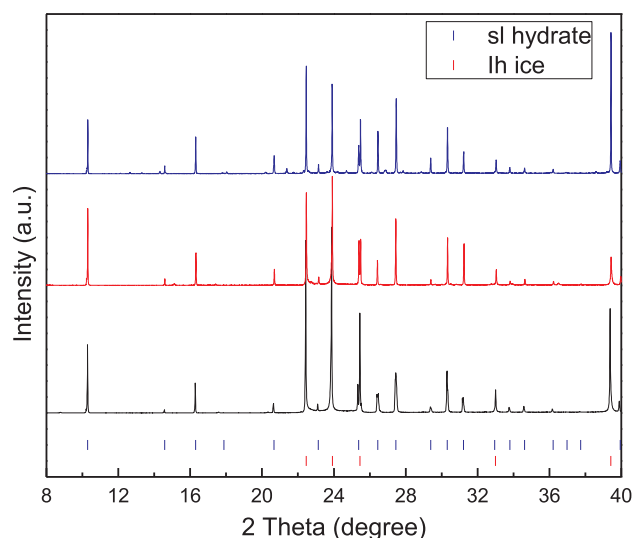


Fig. 1. XRD patterns of R22 hydrates formed in pure water (black line), 5 wt% NaCl (red line), and 5 wt% MgCl₂ (blue line) aqueous solutions. (For interpretation of the references to color in this figure legend, the reader is referred to the web version of this article.)

and all of the patterns indicate the formation of sl hydrate [22]. The blue vertical bars represent some signals from cubic sl hydrate with the space group *Pm3n* and the red vertical bars indicate some peaks corresponding to hexagonal ice (*I_h*).

The lattice parameter and unit cell volume of the R22 hydrates formed in pure water, 5 wt% NaCl, and 5 wt% MgCl₂ aqueous solutions are listed in Table 1. We note that the crystal structure (sl) and lattice parameter ($a = 11.980 \text{ \AA}$) for pure R22 hydrate is almost identical to the results in the previous work (sl and $a = 11.97 \text{ \AA}$) [53].

Raman spectroscopy was used to obtain information on the crystal structure and guest occupation of the R22 hydrates. The Raman spectra of gaseous, liquid, and solid R22 and R22 hydrates formed in the aqueous salt solutions are shown in Figs. 2 and 3. The intramolecular vibration of R22 molecules has been classified into nine vibration modes [50,51]. The Raman bands of the R22 molecules in pure R22 hydrate are identical to those in the R22 hydrates formed in the aqueous salt solutions, as shown in Figs. 2 and 3. The Raman bands of the R22 molecules in the hydrate phases are assigned and listed in Table 2. These results indicate that there are no significant effects of salts, such as NaCl or MgCl₂, on the enclathration of R22 molecules into hydrate cages, or on the hydrate structures.

However, differences in the wavenumbers of the vibration modes for the R22 molecules engaged in the gas hydrate framework can be clearly observed in Figs. 2 and 3. The Raman spectra of R22 molecules in the gas, liquid, and solid phases in Fig. 2 and Table 2 are generally consistent with the Raman results in previous reports [50,51]. In the CF₂ rock region (ν_9), the Raman band of R22 molecules in the liquid and solid phases was observed at 370 cm^{-1} , whereas that of R22 molecules in the gas hydrate was shifted to around 372 cm^{-1} . The two Raman bands in the CF₂ wag region (ν_6) observed in the range of

Table 1

Crystal structure, lattice parameter, and unit cell volume of R22 hydrates with and without salts.

Hydrate	Structure	Space group	Lattice parameter (\AA)	Unit cell volume (\AA^3)
Pure R22	sl	<i>Pm3n</i>	$a = 11.980$	1719.3
R22-NaCl (5 wt %)	sl	<i>Pm3n</i>	$a = 11.965$	1712.9
R22-MgCl ₂ (5 wt %)	sl	<i>Pm3n</i>	$a = 11.972$	1715.9

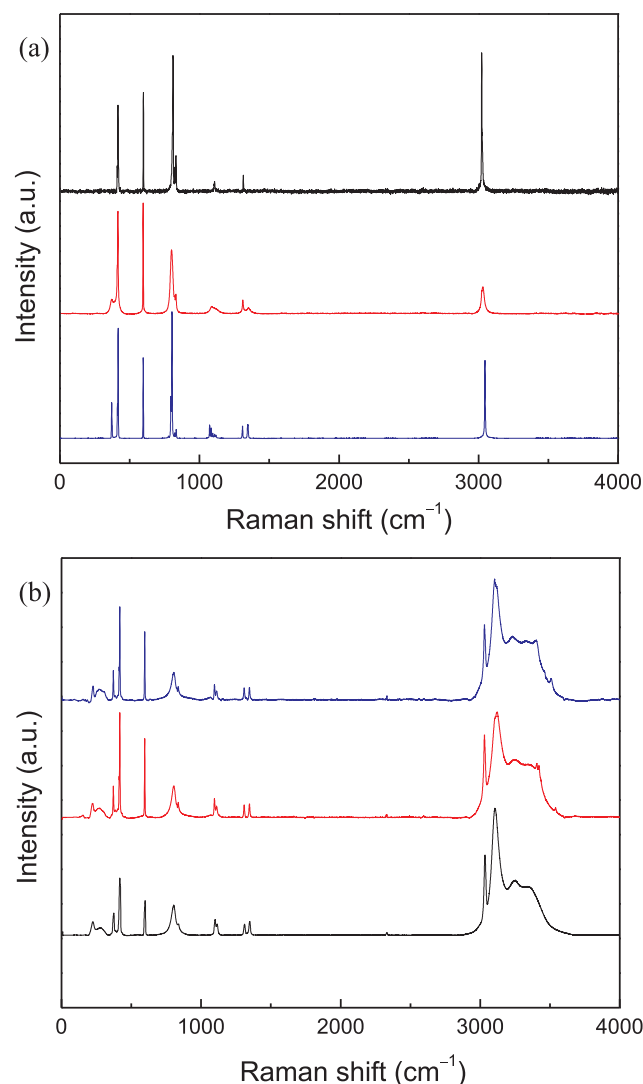


Fig. 2. (a) Raman spectra of R22 gas (black line), liquid (red line), and solid (blue line) measured at 298, 298, and 83 K, respectively. (b) Raman spectra of R22 hydrates formed in pure water (black line), 5 wt% NaCl (red line), and 5 wt % MgCl₂ (blue line) aqueous solutions. (For interpretation of the references to color in this figure legend, the reader is referred to the web version of this article.)

$410\text{--}418 \text{ cm}^{-1}$ are due to isotopes of CH³⁵ClF₂ and CH³⁷ClF₂. The CF₂ scissor vibration in the ν_5 mode was similarly observed as a single peak at 598, 596, 597, and 596 cm^{-1} for the gas, liquid, solid, and hydrate phases, respectively. The effect of Fermi-resonance by the $2\nu_6$ overtone and isotopic species of ³⁵Cl and ³⁷Cl was observed at the C–Cl stretching region (ν_4) of $750\text{--}850 \text{ cm}^{-1}$ (Fig. 3).

A large difference in the shape of Raman bands for the R22 hydrate and solid R22 was observed in the ν_4 spectral region, as shown in Fig. 3. The broad Raman bands at around $\sim 805 \text{ cm}^{-1}$ are due to the C–Cl stretching vibration of R22 molecules engaged in the R22 hydrate, coupled with the Fermi-resonance effect. The Raman bands of the C–F symmetric stretching (ν_3) and CF₂ twist (ν_8) vibrations for the R22 hydrates appear in the spectral region of $1090\text{--}1120 \text{ cm}^{-1}$.

A single Raman band for the HCCL deformation (ν_2) was also observed at around 1309 cm^{-1} for the R22 hydrates. In the C–F asymmetric stretching region (ν_7), the Raman bands were found at the position of 1346 cm^{-1} without any doublet by the isotopes. In particular, we observed a significant change in Raman signals at around 3050 cm^{-1} for the C–H stretching vibration (ν_1) mode (Fig. 3). For the ν_1 vibration mode, the Raman band of the R22 molecules engaged in the

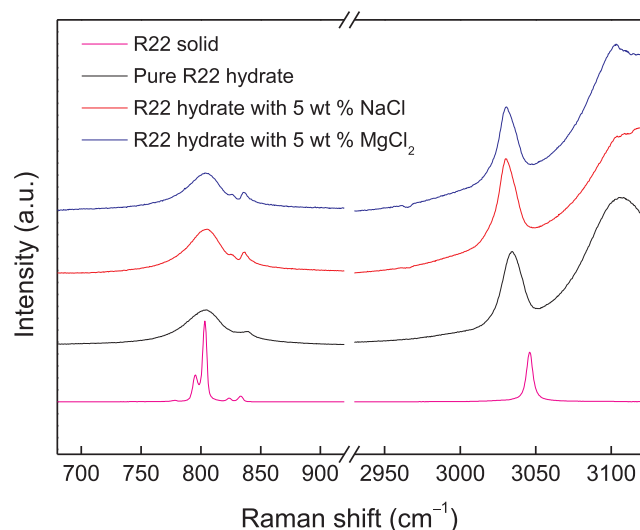


Fig. 3. Raman spectra in the ν_1 and ν_4 spectral regions of R22 solid and hydrates.

Table 2
Vibration mode of R22 molecules in gas, liquid, solid, and hydrates.

Assignment ^a	Wavenumber (cm^{-1})					
	Gas (298 K)	Liquid (298 K)	Solid (83 K)	Pure R22 hydrate (83 K)	R22 hydrate-NaCl (83 K)	R22 hydrate-MgCl ₂ (83 K)
ν_9		370	370	372	372	372
ν_6	410	415	412	413	413	413
	416		417	418	418	418
ν_5	598	596	597	596	596	596
$\nu_4 (+2\nu_6)$	811	800	796	805	805	805
	823	821	803	826	826	826
	831	831	823	837	837	837
			833			
ν_3	1108	1086	1073	1096	1096	1096
			1083			
ν_8			1095			
			1108	1112	1112	1112
			1118			
ν_2	1314	1311	1309	1309	1309	1309
ν_7		1352	1345	1346	1346	1346
			1348			
ν_1	3023	3031	3046	3030	3030	3030

^a Lefebvre and Anderson[51].

gas hydrate framework appeared at around 3030 cm^{-1} , while that of R22 molecules in the solid R22 phase could be observed at around 3050 cm^{-1} . The frequency difference between the two Raman bands for the ν_1 vibration mode was $\Delta\nu = 16 \text{ cm}^{-1}$, indicating R22 enclathration in the large cages of the sI hydrate.

Based on the combination of XRD and Raman spectroscopic measurements, we can confirm sI hydrate was formed with and without salts, such as NaCl or MgCl₂, as well as confirm the entrapment of R22 molecules in the large cages of the sI hydrate. Even though R22 hydrates formed in the aqueous salt solutions, there were no significant changes in the crystal structures, lattice parameters, and guest inclusion behaviors of the R22 hydrates, indicating that salts such as NaCl and MgCl₂ do not participate in the gas hydrate framework. As a result, the salts are excluded from the hydrate phases, and enriched-salt phases are concentrated during hydrate formation, which indicates that the HBD technology is a plausible process for producing fresh water from sea

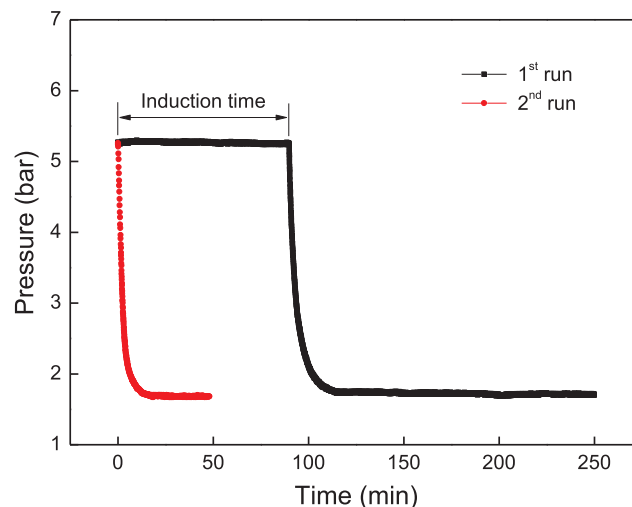


Fig. 4. Formation kinetics of pure R22 hydrate at 278 K.

water.

For HBD technology using the R22 hydrate, the formation kinetics of the R22 hydrate in the presence of salts is important. In addition, aqueous salt concentrations during hydrate formation are constantly changing, and for this reason we investigated the formation kinetics of R22 hydrates in various salt environments.

3.2. Hydrate formation kinetics

Fig. 4 shows the formation kinetics of pure R22 hydrate at 278 K. The 1st run of the formation kinetics of pure R22 hydrate was performed at 278 K and 5.2 bar. The hydrate formation was initiated by vigorously agitating the magnetic drive, followed by a sudden pressure drop, as shown in Fig. 4. Hydrate nucleation is a stochastic process, and the temperature and pressure conditions can affect the induction time for hydrate nucleation [22]. We observed a long induction time for pure R22 hydrate in the 1st run of the kinetic experiment. After the 1st run of the kinetic experiment was completed, the pressure in cell 1 was reduced to atmospheric pressure for hydrate dissociation. After 1 h of the hydrate dissociation process, the 2nd run of the kinetic experiment was repeated using the same procedure. However, we did not observe any induction time for the pure R22 hydrate during the 2nd run of the kinetic experiment due to the memory effect [54,55]. To eliminate the effect of induction time on hydrate formation, we modified our experimental procedure, as described above (see Section 2). It should be noted that fast hydrate nucleation is an important criteria for the development of practical HBD technology.

All of the R22 hydrate formation kinetics experiments in the presence of salts were performed using the modified experimental procedure. As shown in Figs. 5 and 6, no induction time for R22 hydrate formation was observed in either the 1st or 2nd run of the kinetic experiments when the modified experimental procedure was applied.

Fig. 5 shows the formation kinetics of the R22 hydrate in the NaCl aqueous solution system (pure water, black; 5 wt% NaCl solution, red; 10 wt% NaCl solution, blue) and R22 hydrate in the MgCl₂ aqueous solution system (pure water, black; 5 wt% MgCl₂ solution, red; 10 wt% MgCl₂ solution, blue), respectively. After the R22 hydrate starts to nucleate, the system pressure rapidly decreases. As shown in Fig. 5, the initial formation rate of the R22 hydrates decreases as the concentration of salts increases, resulting in a reduction in the final pressure at steady state. Clearly, the final pressure in hydrate formation is closely related to the three-phase equilibrium pressure.

The formation of R22 hydrate in pure water was almost completed in 500 s, and the final system pressure was about 1.86 bar. In a previous study by Barduhn and Lee [47], the phase equilibrium conditions of

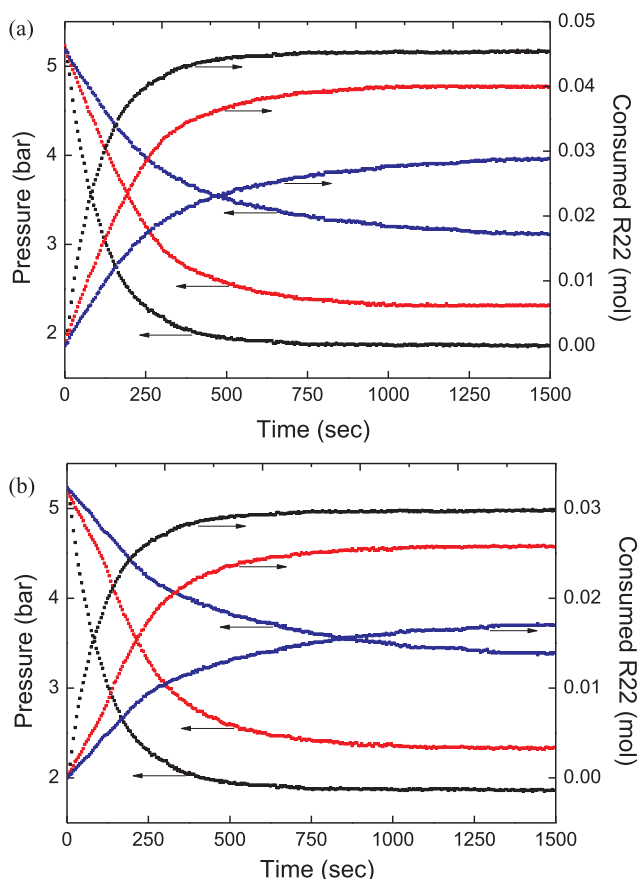


Fig. 5. (a) Formation kinetics of R22 hydrate in pure water (black), 5 wt% (red), and 10 wt% (blue) NaCl aqueous solutions at 278 K. (b) Formation kinetics of R22 hydrate in pure water (black), 5 wt% (red), and 10 wt% (blue) MgCl₂ aqueous solutions at 278 K. (For interpretation of the references to color in this figure legend, the reader is referred to the web version of this article.)

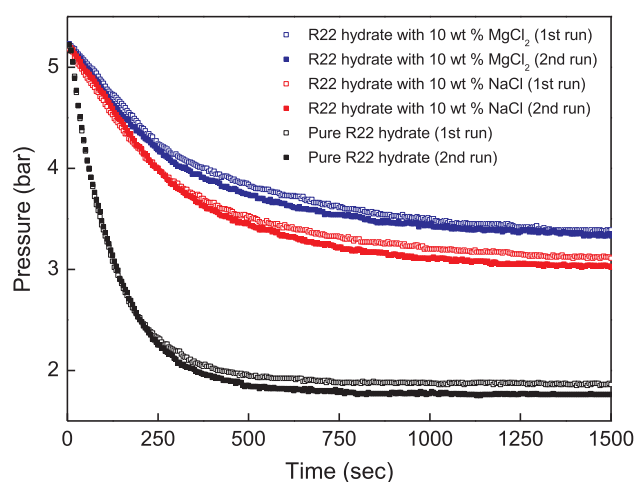


Fig. 6. Memory effect on the R22 hydrate formation in aqueous salt solutions. The second runs were performed at 1 h after dissociation of R22 hydrate formed from the first runs.

pure R22 hydrate were measured. They reported the pressure (P) and temperature (T) correlation function for the phase equilibrium conditions of pure R22 hydrate. Based on their equation, the equilibrium pressure of pure R22 hydrate at 278 K is calculated to be 1.65 bar. Therefore, we can expect that the hydrate formation in our experimental system (at constant temperature and constant volume) is

apparently completed at a steady state pressure which is slightly higher than the equilibrium pressure.

After the 1st run of the kinetic experiment, the system pressure decreased to atmospheric pressure, and the first formed hydrate was dissociated for 1 h. Then, the hydrate formation experiment was repeated again (2nd run). As shown in Fig. 6, the growth rate of pure R22 hydrate formation in the 1st and 2nd run of the kinetic experiments is quite similar; the final system pressure was about 1.78 bar for the 2nd run of the kinetic experiments. It is interesting to note that this value is slightly lower than that for the 1st run, and still higher than the equilibrium pressure. Similar behavior was also observed for the formation of R22 hydrates in the 10 wt% NaCl and MgCl₂ solutions, as shown in Fig. 6.

As we know, the equilibrium boundary for R22 hydrate in the presence of salt solutions is shifted to higher pressure and lower temperature regions as the concentration of salts in the aqueous solution increases [44]. Therefore, the formation rate of R22 hydrates absolutely depends on the salinity in solution because it shifts the equilibrium boundary, accompanied by changes in the sub-cooling temperature.

The initial growth rate (r^{ini} , mol s⁻¹) of the R22 hydrates in the presence of salts can be estimated from the formation kinetics. As shown in Table 3, the initial growth rate of pure R22 hydrate is calculated to be 2.1933×10^{-4} mol s⁻¹. Assuming that the R22 molecules fully occupy only the large cages of the sI hydrate, the theoretical hydrate number is about 7.67. When considering this value and the volume of the hydrate reactor, the rate of water production by hydrate formation is estimated to be 6.0705×10^{-4} mol-H₂O s⁻¹ L⁻¹. For 5 wt% NaCl and 5 wt% MgCl₂ solutions, the rate of pure water production is estimated to be 2.7063×10^{-4} and 1.8270×10^{-4} mol-H₂O s⁻¹ L⁻¹, respectively. These values are comparable to that reported for HFC-32 (difluoromethane) hydrate formation with 5 wt% NaCl solution at 283 K (1.4×10^{-4} mol-H₂O s⁻¹ L⁻¹) [56].

As expected, the production rate of pure water decreases with increasing salinity, which is obviously due to the inhibition effect of salts on hydrate formation. In addition, the equilibrium pressure of the R22 hydrate in the presence of salts is shifted to higher pressure conditions, and thus the amount of R22 consumed by hydrate formation also becomes smaller in the presence of salts. This clearly results in a reduction in the total amount of pure water produced by hydrate formation in the presence of salts.

As shown in Fig. 5 and Table 3, both the initial formation rate and the final pressure of the R22 hydrate in the MgCl₂ solutions are smaller than those in NaCl solutions. This indicates that the inhibition effect of MgCl₂ on R22 hydrate formation is stronger than that of NaCl. This may also be caused by the higher ionic strength of MgCl₂ solutions. Interestingly, the difference in the initial formation rate between the 1st and 2nd runs is marginal, even though there is a slightly larger formation of R22 hydrate in the 2nd runs.

3.3. Kinetics model

Normally, hydrate growth is affected by three major correlations: intrinsic growth kinetics, mass transfer limitation, and heat transfer limitation [22]. In our experimental systems, vigorous agitation using the magnetic drive at a stirring rate of 400 rpm allows the mass transfer limitation problem to be neglected. In addition, a sufficient cooling system and vigorous agitation can also resolve the heat transfer limitation problem. Therefore, we assume that the growth of our R22 hydrate in the presence of salt solutions is limited only by the intrinsic growth kinetics.

Assuming that the system pressure P is directly proportional to the amount of consumed R22 molecules, it can be expressed as follows.

$$-\frac{dP}{dt} = k'(P - P_{\text{eq}}) \quad (1)$$

where P_{eq} is the final equilibrium pressure at the end of the kinetic runs,

Table 3
Kinetic parameters for formation of R22 hydrates with and without salts.

Hydrate system	T (K)	P_0 (MPa)	P_{eq} (MPa)	Time scale used for fitting (s)	$\hat{k} \times 10^3$ (s^{-1})	$r^{mi} \times 10^4$ ($mol\ s^{-1}$)	$k_{app} \times 10^4$ ($mol\ s^{-1}\ MPa^{-1}$)
Pure R22	278	0.521	0.186	0–460	7.7989	2.1933	7.5965
R22 + 5 wt% NaCl	278	0.523	0.232	0–600	4.9288	0.9778	4.9188
R22 + 10 wt% NaCl	278	0.518	0.311	0–700	3.2471	0.5533	3.3907
R22 + 5 wt% $MgCl_2$	278	0.520	0.234	0–600	4.7388	0.6601	4.7295
R22 + 10 wt% $MgCl_2$	278	0.523	0.339	0–700	2.8553	0.3851	3.0507

and k' is the first-order reaction rate constant. Integrating the above equation with t gives

$$-\ln\left(\frac{P-P_{eq}}{P_0-P_{eq}}\right) = k't \quad (2)$$

This approach is almost identical to the reaction kinetic model determined by using the time variation of system pressure at high agitation intensities, as proposed in a previous work [57]. This also indicates that diffusion resistance is nearly eliminated at a high agitation speed, and thus the intrinsic reaction is rate controlling. The reaction rate constant k' can be determined using Eq. (2) and the initial slope of pressure changes, as shown in Fig. 7a. Here, we only considered the initial period of the hydrate growth stage, governing the linearity.

In Table 3, the values of k' and the time scale used for fitting the pressure change data were tabulated. When using the values of k' and Eq. (2), the calculated time-dependent pressure profile was in a good agreement with the experimental results as shown in Fig. 7b.

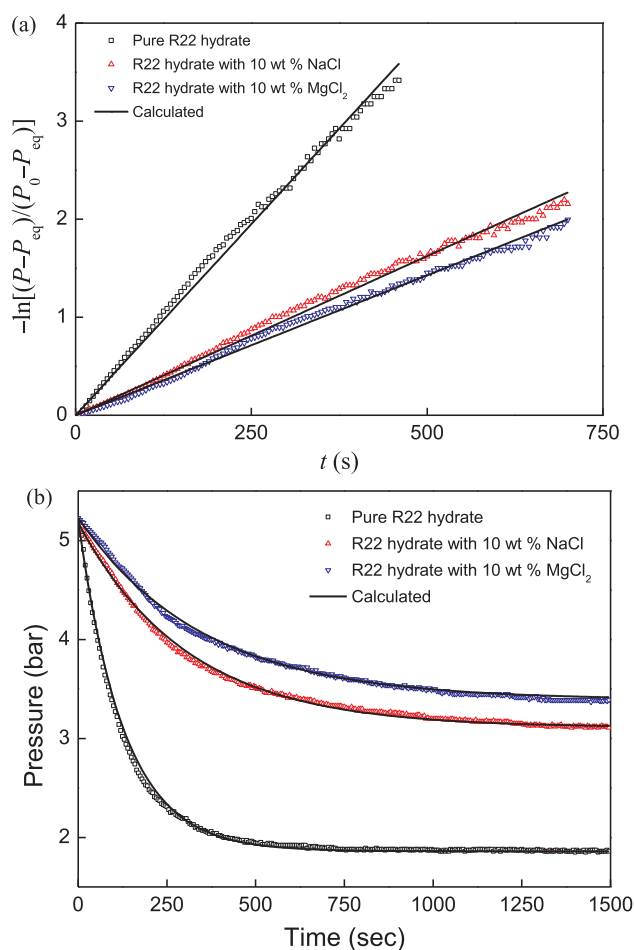


Fig. 7. (a) Plot of the fitting results of experimental data in the initial formation reaction of R22 hydrates with and without salts. (b) Formation kinetics of R22 hydrates with and without salts. Solid lines are the calculated results.

Based on the hydrate growth kinetic model proposed by Englezos et al. [58], the reaction rate $r(t)$ can also be expressed as:

$$r(t) = \frac{dn}{dt} = k_{app}(f - f_{eq}) \quad (3)$$

where n is the mole number of consumed R22, f is the fugacity of R22 in the gas phase, f_{eq} is the equilibrium fugacity of R22 at the end of runs, and k_{app} is the apparent rate constant. This equation has been used for estimating the formation kinetics of refrigerant hydrates [59] and methane hydrate in surfactant solutions [60]. In general, the fugacity is expressed as a function of pressure deviated from the ideality by introducing the fugacity coefficient ϕ .

$$f = P\phi \quad (4)$$

In the present study, we used the Soave-Redlich-Kwong equation of state for calculating the fugacity coefficient as follows [61].

$$\ln \phi = \ln \frac{RT}{P(v-b)} - \frac{a}{bRT} \ln \left(\frac{v+b}{v} \right) + Z-1 \quad (5)$$

Using $P(t)$ from Eq. (2) and $\phi(t)$ from Eq. (5), the fugacity $f(t)$ can be obtained as a function of time. Previously, the apparent rate constant at a specific time was calculated by observing the instantaneous reaction rate at the beginning time of hydrate growth [58–60]. However, there are many uncertainties at the beginning time of hydrate growth, such as heterogeneous crystal growth, abrupt temperature and pressure variation, and stochastic induction time.

Fig. 8 shows changes in the temperature during the formation reaction of pure R22 hydrate. The cell temperature rapidly increases in the initial stage to a maximum at ~ 100 s and then gradually decreases with increasing time to the initial cell temperature. This is definitely caused by the exothermic nature of the gas hydrate formation reaction, leading to possible errors in calculating the apparent rate constant at the beginning time. To overcome this problem, we provide a new approach using the integration method. Assuming that the apparent rate constant is nearly constant during hydrate formation, it can easily be obtained by integrating Eq. (3).

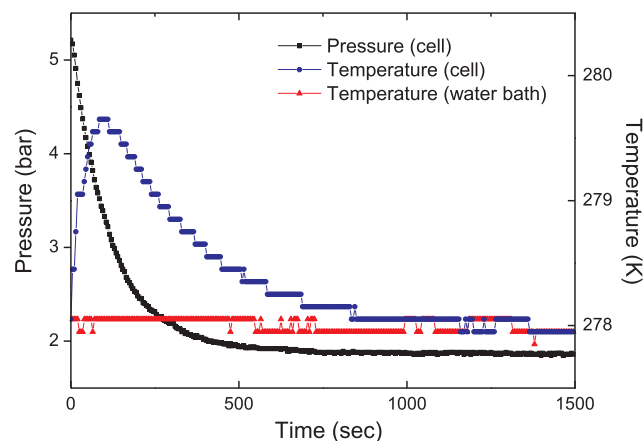


Fig. 8. Change in temperature and pressure during R22 hydrate formation at an initial pressure and temperature of 5.21 bar and 278 K.

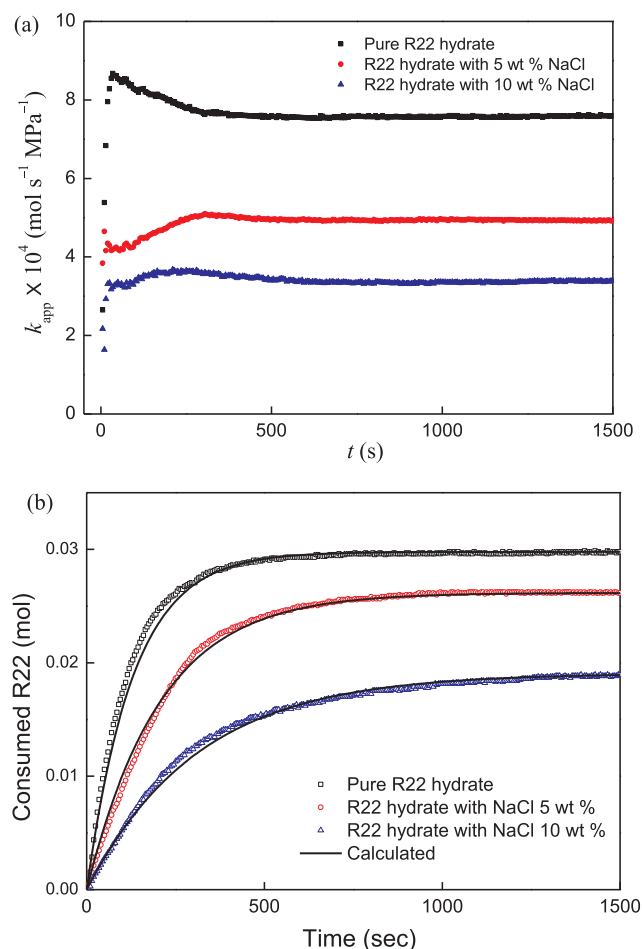


Fig. 9. (a) Apparent rate constant as a function of time during formation of R22 hydrates with and without NaCl. (b) Comparison of experimental and calculated formation kinetics of R22 hydrates with and without NaCl.

$$k_{app} = \frac{n(t)}{\int_0^t [P(t)\phi(t) - P_{eq}\phi_{eq}] dt} \quad (6)$$

This equation only requires the mole number of R22 consumed (experimentally measured) and the non-linear integration of the fugacity function at a specific time.

To check our approximation, we represented the time-dependent behavior of k_{app} calculated using Eq. (6) and the experimental data for the mole number of consumed R22. As shown in Fig. 9a, the apparent rate constant rapidly increases in the initial stage, up to ~40 s, and then it is stabilized at ~300 s with a steady state value. It has been reported that the increase in k_{app} at the beginning is due to the increased number of hydrate particles [60].

The calculated values of k_{app} at the steady state are listed in Table 3. For pure R22 hydrate, the apparent rate constant k_{app} is calculated to be 7.5965×10^{-4} mol s⁻¹ MPa⁻¹ at 278 K. When considering the amount of water used, it stands for 1.5193×10^{-4} mol-gas/mol-H₂O s⁻¹ MPa⁻¹. This value has a similar order of magnitude compared to those for R407C (2.75×10^{-4} mol-gas/mol-H₂O s⁻¹ MPa⁻¹ at 281.8 K and 7.3 bar) and R507C hydrate formations (0.8333×10^{-4} mol-gas/mol-H₂O s⁻¹ MPa⁻¹ at 279.9 K and 7.5 bar) [59]. Using all the calculated values of k_{app} (Table 3), the amount of R22 consumed during hydrate formation can be predicted as a function of time. As shown in Fig. 9b, the predicted results are in a good agreement with the experimental kinetics, even though there is a slight deviation at the initial stage.

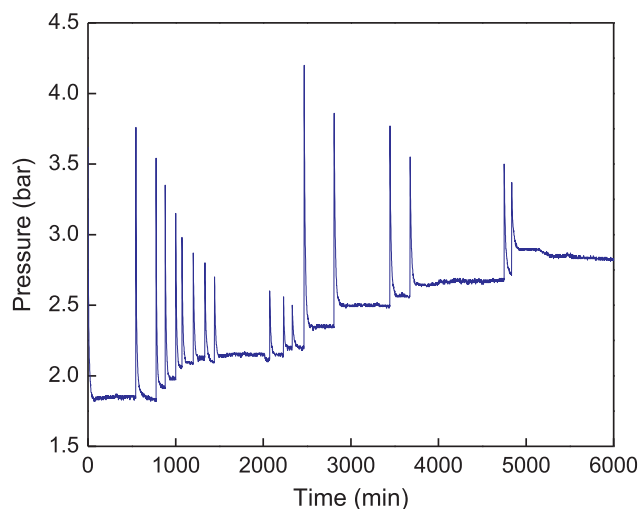


Fig. 10. Multi-stage formation of R22 hydrate in 10 wt% NaCl aqueous solution at 274 K.

3.4. Multi-stage desalination process

Fig. 10 shows the formation of R22 hydrate in the presence of 10 wt % NaCl solution at 274 K. R22 gas is liquefied at pressures above 5.12 bar at 274 K [52]. Thus, multi-stage hydrate formation was performed by injecting R22 gas in a series to obtain high hydrate yields, as shown in Fig. 10. As mentioned in the previous section, the growth of R22 hydrate in the presence of salts is only limited by intrinsic growth kinetics. Therefore, hydrate formation in each stage finished after reaching an equilibrium pressure, in 200 min, following vigorous agitation. In addition, salts were excluded from the hydrate phase and the enriched-salt phase was concentrated during hydrate formation, resulting in changes in the equilibrium pressure. As each stage progressed, the equilibrium pressure gradually increased, as shown in Fig. 10. This is a clear indication of the increase in salt concentration in the aqueous phase.

At the final stage, the Cl⁻ concentration in the liquid phase was determined using ion chromatography, which indicated that the salt solution with an initial concentration of 10 wt% NaCl had changed to 18.9 wt% NaCl aqueous solution due to the formation of the gas hydrate. This also indicates that 52% (water recovery) of the water in the aqueous salt solution was converted to R22 hydrate by the multi-stage HBD process. Combined with the separation of the R22 hydrate from the concentrated salt solution, the regasification process should be considered to obtain fresh water from the R22 hydrate.

3.5. Proposed process of hydrate-based desalination using R22 hydrate

Fig. 11 represents the proposed diagram of hydrate-based desalination using R22 hydrate. This conceptual process of hydrate-based desalination technology can be divided into three sections; (1) hydrate formation stage, (2) hydrate separation stage, and (3) hydrate decomposition stage (Fig. 11). This study focuses on the hydrate formation stage, and the key findings can be addressed as follow; (1) salts cannot participate in the hydrate framework, (2) aqueous salt concentrations during hydrate formation are constantly changed, (3) the hydrate formation kinetics can be significantly affected by the concentration of the salt solutions, (4) a new kinetic model for theoretically predicting the formation kinetics of gas hydrates in salt environments is established. Higher hydrate conversion indicates more fresh-water recovery, and thus; the continuous injection of hydrate-forming agent (R22 gas) is an important parameter for the development of HBD process during hydrate formation stage.

In the hydrate separation stage, a small amount of salt ions may

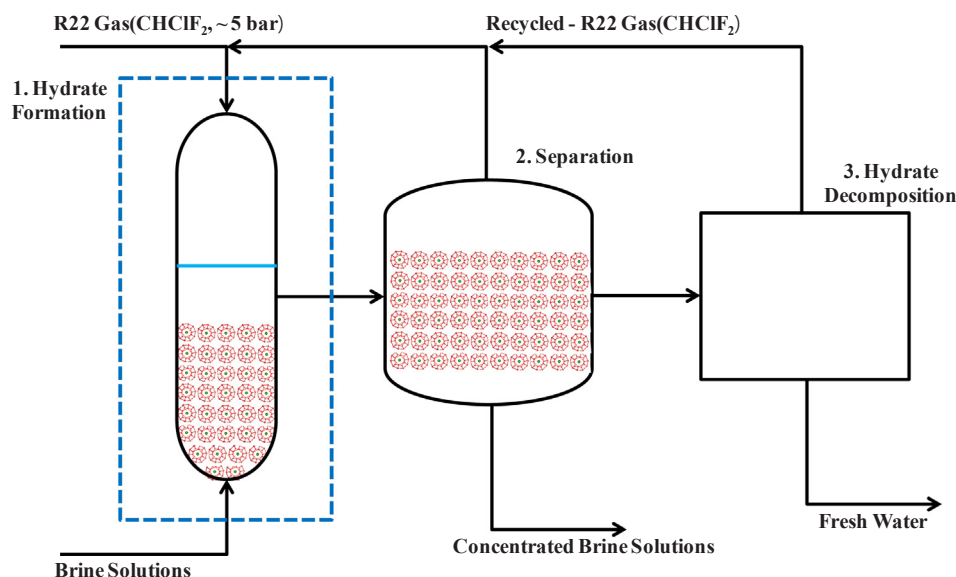


Fig. 11. Schematic process diagram of hydrate-based desalination using R22 hydrate.

remains in the grain boundary phase between hydrate-solid crystals. Therefore, post-hydrate treatment processes should be considered in stage 2 (Fig. 11). Han et al. [62,63] reported that filtration, washing, centrifuging, and sweating treatments of hydrate crystal could enhance the salt rejection percentage (salt removal). The effect of post-treatment on the salt rejection in desalination by R22 hydrates should be identified in future studies. In addition, depressurization or thermal stimulation method can be applied for hydrate decomposition process to obtain fresh-water. Especially, R22 gas is considered as ozone depleting materials as well as greenhouse gases. Therefore, it is necessary to take into account a careful recycle of R22 gas in the desalination process.

Badu et al. [64] reported that two major parameters of water recovery and energy consumption are crucial for practical application of HBD process and HBD process has following advantages in comparison with other conventional desalination technologies such as reverse osmosis (RO) and multi-stage flash distillation (MSF); (1) typical water recovery in MSF is up to 20%, but HBD process can show higher water recovery (52% water recovery in this study), (2) RO technology is usually operated at pressures of 50–80 bar, but HBD process using R22 hydrate can be operated at pressure of 5 bar, (3) energy consumption for HBD process can be dramatically reduced by utilizing LNG waste cold energy [65].

There are still many challenges for commercialization of HBD process for fresh-water recovery, zero liquid discharge, and heavy metal separation from aqueous salt solutions. The present study provides useful insights for separating ionic compounds from aqueous solutions by hydrate-based separation processes.

4. Conclusions

In this study, we identified the crystal structure and guest inclusion behavior of R22 hydrates in the presence of salts, NaCl and MgCl₂. Even though R22 hydrates were formed in the aqueous salt solutions, there were no significant changes in the crystal structure and guest inclusion behavior of the resulting R22 hydrates. This clearly indicates that salts such as NaCl and MgCl₂ do not participate in the gas hydrate framework.

To monitor the hydrate formation kinetics in various salt environments, we investigated the formation kinetics of R22 hydrates in the presence of 5 wt% NaCl, 10 wt% NaCl, 5 wt% MgCl₂, and 10 wt% MgCl₂. We confirmed that the hydrate formation kinetics can be significantly affected by the concentration of the salt solutions.

Finally, the multi-stage formation of R22 hydrates in the presence of 10 wt% NaCl solution at 274 K revealed that the equilibrium pressure of the R22 hydrates in the presence of salts gradually increases with each progressive stage, leading to high hydrate yields and increased salt concentration in the brine solutions. This study provides key parameters for developing the HBD technology.

Acknowledgements

This research was supported by the Mid-career Research Program (2015003772) through the National Research Foundation of Korea (NRF) grant funded by the Ministry of Science and ICT. High-resolution synchrotron XRD measurements were performed at the beamline 9B of the Pohang Accelerator Laboratory (PAL).

References

- [1] C.J. Vörösmarty, P. Green, J. Salisbury, R.B. Lammers, Global water resources: vulnerability from climate change and population growth, *Science* 289 (2000) 284–288.
- [2] C.W. Howe, F.P. Linaweaver, The impact of price on residential water demand and its relation to system design and price structure, *Water Resour. Res.* 3 (1967) 13–32.
- [3] T. Oki, S. Kanae, Global hydrological cycles and world water resources, *Science* 313 (2006) 1068–1072.
- [4] S.M. Olmstead, W.M. Hanemann, R.N. Stavins, Water demand under alternative price structures, *J. Environ. Econom. Manage.* 54 (2007) 181–198.
- [5] M. Elimelech, W.A. Phillip, The future of seawater desalination: energy, technology, and the environment, *Science* 333 (2011) 712–717.
- [6] A.D. Khawaji, I.K. Kutubkhanah, J.M. Wie, Advances in seawater desalination technologies, *Desalination* 221 (2008) 47–69.
- [7] M.A. Shannon, P.W. Bohn, M. Elimelech, J.G. Georgiadis, B.J. Mariñas, A.M. Mayes, Science and technology for water purification in the coming decades, *Nature* 452 (2007) 301–310.
- [8] I.C. Karagiannis, P.G. Soldatos, Water desalination cost literature: review and assessment, *Desalination* 223 (2008) 448–456.
- [9] C. Fritzmann, J. Löwenberg, T. Wintgens, T. Melin, State-of-the-art of reverse osmosis, *Desalination* 216 (2007) 1–76.
- [10] B. Peñate, L. García-Rodríguez, Current trends and future prospects in the design of seawater reverse osmosis desalination technology, *Desalination* 284 (2012) 1–8.
- [11] Z.R. Chong, S.H.B. Yang, P. Babu, P. Linga, X.S. Li, Review of natural gas hydrates as an energy resource: prospects and challenges, *Appl. Energy* 162 (2016) 1633–1652.
- [12] S.H.B. Yang, P. Babu, S.F.S. Chua, P. Linga, Carbon dioxide hydrate kinetics in porous media with and without salts, *Appl. Energy* 162 (2016) 1131–1140.
- [13] Z.R. Chong, Z. Yin, J.H.C. Tan, P. Linga, Experimental investigations on energy recovery from water-saturated hydrate bearing sediments via depressurization approach, *Appl. Energy* 204 (2017) 1513–1525.
- [14] Z.R. Chong, G.A. Pujar, M. Yang, P. Linga, Methane hydrate formation in excess water simulating marine locations and the impact of thermal stimulation on energy recovery, *Appl. Energy* 177 (2016) 409–421.

- [15] W. Kondo, K. Ohtsuka, R. Ohmura, S. Takeya, Y.H. Mori, Clathrate-hydrate formation from a hydrocarbon gas mixture: compositional evolution of formed hydrate during an isobaric semi-batch hydrate-forming operation, *Appl. Energy* 113 (2014) 864–871.
- [16] T. Ogawa, T. Ito, K. Watanabe, K. Tahara, R. Hiraoka, J. Ochiai, et al., Development of a novel hydrate-based refrigeration system: a preliminary overview, *Appl. Therm. Eng.* 26 (2006) 2157–2167.
- [17] T. Uchida, M. Moriwaki, S. Takeya, I.Y. Ikeda, R. Ohmura, J. Nagao, et al., Two-step formation of methane–propane mixed gas hydrates in a batch-type reactor, *AIChE J.* 50 (2004) 518–523.
- [18] Q.N. Lv, X.S. Li, Z.Y. Chen, Formation of cyclopentane-methane hydrates in brine systems and characteristics of dissolved ions, *Appl. Energy* 184 (2016) 482–490.
- [19] J.C. Feng, Y. Wang, X.S. Li, Z.Y. Chen, Y. Zhang, Investigation into optimization condition of thermal stimulation for hydrate dissociation in the sandy reservoir, *Appl. Energy* 154 (2015) 995–1003.
- [20] Z.M. Xia, X.S. Li, Z.Y. Chen, G. Li, J. Cai, Hydrate-based CO₂ capture and CH₄ purification from simulated biogas with synergic additives based on gas solvent, *Appl. Energy* 162 (2016) 1153–1159.
- [21] Y. Wang, X.S. Li, G. Li, Y. Zhang, Z.Y. Chen, Experimental investigation into methane hydrate production during three-dimensional thermal stimulation with five-spot well system, *Appl. Energy* 110 (2013) 90–97.
- [22] E.D. Sloan, *Clathrate Hydrates of Natural Gases*, second ed., Marcel Dekker, New York, 1988.
- [23] E.D. Sloan, Fundamental principles and applications of natural gas hydrates, *Nature* 426 (2003) 353–363.
- [24] J.S. Gudmundsson, M. Parlaktuna, A.A. Khokhar, Storing natural gas as frozen hydrate, *SPE Prod. Facilities* 9 (1994) 69–73.
- [25] H.P. Veluswamy, A. Kumar, R. Kumar, P. Linga, An innovative approach to enhance methane hydrate formation kinetics with leucine for energy storage application, *Appl. Energy* 188 (2017) 190–199.
- [26] Z. Sun, R. Wang, R. Ma, K. Guo, S. Fan, Natural gas storage in hydrate with the presence of promoters, *Energy Convers. Manage.* 44 (2003) 2733–2742.
- [27] H. Ogawa, N. Imura, T. Miyoshi, R. Ohmura, Y.H. Mori, Thermodynamic simulations of isobaric hydrate-forming operations for natural gas storage, *Energy Fuels* 23 (2009) 849–856.
- [28] P. Linga, R. Kumar, P. Englezos, The clathrate hydrate process for post and pre-combustion capture of carbon dioxide, *J. Hazard. Mater.* 149 (2007) 625–629.
- [29] P. Linga, R. Kumar, P. Englezos, Gas hydrate formation from hydrogen/carbon dioxide and nitrogen/carbon dioxide gas mixtures, *Chem. Eng. Sci.* 62 (2007) 4268–4276.
- [30] C.G. Xu, X.S. Li, Research progress of hydrate-based CO₂ separation and capture from gas mixtures, *RSC Adv.* 4 (2014) 18301–18316.
- [31] S.P. Kang, H. Lee, Recovery of CO₂ from flue gas using gas hydrate: thermodynamic verification through phase equilibrium measurements, *Environ. Sci. Technol.* 34 (2000) 4397–4400.
- [32] J. Zheng, P. Zhang, P. Linga, Semiclathrate hydrate process for pre-combustion capture of CO₂ at near ambient temperatures, *Appl. Energy* 194 (2017) 267–278.
- [33] Y. Yang, D. Shin, S. Choi, Y. Woo, J.W. Lee, D. Kim, et al., Selective encaging of N₂O in N₂O–N₂ binary gas hydrates via hydrate-based gas separation, *Environ. Sci. Technol.* 51 (2017) 3550–3557.
- [34] J.W. Lee, J. Poudel, M. Cha, S.J. Yoon, J.H. Yoon, Highly selective CO₂ extraction from a mixture of CO₂ and H₂ gases using hydroquinone clathrates, *Energy Fuels* 30 (2016) 7604–7609.
- [35] S. Tomita, S. Akatsu, R. Ohmura, Experiments and thermodynamic simulations for continuous separation of CO₂ from CH₄ + CO₂ gas mixture utilizing hydrate formation, *Appl. Energy* 146 (2015) 104–110.
- [36] S. Akatsu, S. Tomita, Y.H. Mori, R. Ohmura, Thermodynamic simulations of hydrate-based removal of carbon dioxide and hydrogen sulfide from low-quality natural gas, *Ind. Eng. Chem. Res.* 52 (2013) 15165–15176.
- [37] Z.M. Xia, X.S. Li, Z.Y. Chen, G. Li, C.G. Xu, Hydrate-based acidic gases capture for clean methane with new synergic additives, *Appl. Energy* 162 (2016) 1153–1159.
- [38] J. Cai, C. Xu, Z. Xia, Z. Chen, X. Li, Hydrate-based methane recovery from coal mine methane gas in scale-up equipment by bubbling, *Energy Procedia* 105 (2017) 4983–4989.
- [39] Y. Seo, D. Moon, C. Lee, J.W. Park, B.S. Kim, G.W. Lee, et al., Equilibrium, kinetics, and spectroscopic studies of SF₆ hydrate in NaCl electrolyte solution, *Environ. Sci. Technol.* 49 (2015) 6045–6050.
- [40] J. Javanmardi, M. Moshfeghian, Energy consumption and economic evaluation of water desalination by hydrate phenomenon, *Appl. Therm. Eng.* 23 (2003) 845–857.
- [41] K.N. Park, S.Y. Hong, J.W. Lee, K.C. Kang, Y.C. Lee, M.G. Ha, et al., A new apparatus for seawater desalination by gas hydrate process and removal characteristics of dissolved minerals (Na⁺, Mg²⁺, Ca²⁺, K⁺, B³⁺), *Desalination* 274 (2011) 91–96.
- [42] *The Montreal Protocol on Substances that Deplete the Ozone Layer*, UNEP, ISBN 92-807-1888-6, 2000.
- [43] G. Siegemund, W. Schwertfeger, A. Feiring, B. Sart, F. Behr, H. Vogel, et al., *Fluorine Compounds, Organic*, Ullmann's Encyclopedia of Industrial Chemistry, Wiley-VCH, Weinheim, 2002.
- [44] M.K. Chun, H. Lee, B.J. Ryu, Phase equilibria of R22 (CHClF₂) hydrate systems in the presence of NaCl, KCl, and MgCl₂, *J. Chem. Eng. Data* 45 (2000) 1150–1153.
- [45] M.K. Chun, J.H. Yoon, H. Lee, Clathrate phase equilibria for the water + deuterium oxide + carbon dioxide and water + deuterium oxide + chlorodifluoromethane (R22) Systems, *J. Chem. Eng. Data* 41 (1996) 1114–1116.
- [46] M.K. Chun, H. Lee, Phase equilibria of R22 (CHClF₂) hydrate system in the presence of sucrose, glucose and lactic acid, *Fluid Phase Equilib.* 150 (1998) 361–370.
- [47] A.J. Bardukn, W.C. Lee, Thermodynamic properties of F-22 (CHClF₂) hydrate for use in desalting, *Desalination* 25 (1978) 151–162.
- [48] K. Maeda, Y. Katsura, Y. Asakuma, K. Fukui, Concentration of sodium chloride in aqueous solution by chlorodifluoromethane gas hydrate, *Chem. Eng. Process* 47 (2008) 2281–2286.
- [49] M. Karamoddin, F. Varaminian, M. Daraee, Kinetic study on the process of CHClF₂ (R22) hydrate formation in the presence of SDS surfactant based on chemical affinity, *J. Nat. Gas Sci. Eng.* 19 (2014) 46–51.
- [50] J.V. Magill, K.M. Gough, W.F. Murphy, The vibrational spectrum and normal coordinate analysis of chlorodifluoromethane, CHClF₂, *Spectrochim. Acta A* 42 (1986) 705–715.
- [51] J.H. Lefebvre, A. Anderson, Raman study of a phase transition in solid chlorodifluoromethane, *J. Raman Spectrosc.* 23 (1992) 243–247.
- [52] *NIST Chemistry WebBook* (<http://webbook.nist.gov/chemistry/>).
- [53] T.A. Wittstruck, W.S. Brey, A.M. Buswell, W.H. Rodebush, Solid hydrates of some halomethanes, *J. Chem. Eng. Data* 6 (1961) 343–346.
- [54] D.L. Sun, Reaction mechanism between “memory effect” and induction time of gas hydrate formation, *J. Coal Sci. Eng.* 14 (2008) 280–282.
- [55] Q. Wu, B. Zhang, Memory effect on the pressure-temperature condition and induction time of gas hydrate nucleation, *J. Nat. Gas Chem.* 19 (2010) 446–451.
- [56] R.W. Bradshaw, J.A. Greathouse, R.T. Cygan, B.A. Simmons, D.E. Dedrick, E.H. Majzoub, *Desalination Utilizing Clathrate Hydrates (LDRD Final Report)*, Sandia Report 2008, SAND2007-6565.
- [57] B. ZareNezhad, V. Montazeri, Development of a high efficient gas to hydrate (GTH) conversion process using SDS kinetic promoter for maximizing the CO₂ recovery with minimum energy consumption, *Energy Convers. Manage.* 79 (2014) 289–293.
- [58] P. Englezos, P. Dholabhai, N. Kapgeralos, P.R. Bishnoi, Kinetics of formation of methane and ethane gas hydrates, *Chem. Eng. Sci.* 42 (1987) 2647–2658.
- [59] H. Hashemi, S. Babae, A.H. Mohammadi, P. Naidoo, D. Ramjugernath, Experimental study and modeling of the kinetics of refrigerant hydrate formation, *J. Chem. Thermodyn.* 82 (2015) 47–52.
- [60] J.S. Zhang, S. Lee, J.W. Lee, Kinetics of methane hydrate formation from SDS solution, *Ind. Eng. Chem. Res.* 46 (2007) 6353–6359.
- [61] G. Soave, Equilibrium constants from a modified Redlich-Kwong equation of state, *Chem. Eng. Sci.* 27 (1972) 1197–1203.
- [62] S. Han, J.Y. Shin, Y.W. Rhee, S.P. Kang, Enhanced efficiency of salt removal from brine for cyclopentane hydrates by washing, centrifuging, and sweating, *Desalination* 354 (2014) 17–22.
- [63] S. Han, Y.W. Rhee, S.P. Kang, Investigation of salt removal using cyclopentane hydrate formation and washing treatment for seawater desalination, *Desalination* 404 (2017) 132–137.
- [64] P. Badu, A. Nambiar, T. He, I.A. Karimi, J.D. Lee, P. Englezos, P. Linga, A review of clathrate hydrate based desalination to strengthen energy – water nexus, *ACS Sustain. Chem. Eng.* 6 (2018) 8093–8107, <https://doi.org/10.1021/acssuschemeng.8b01616>.
- [65] T. He, S.K. Nair, P. Babu, P. Linga, I.A. Karimi, A novel conceptual design of hydrate based desalination (HyDesal) process by utilizing LNG cold energy, *Appl. Energy* 222 (2018) 13–24.